Nano Research

Open Access

Communication

Platelet-derived purified exosome product (PEP): A clinical-grade lyophilized extracellular vesicle product with broad therapeutic potential, including kidney repair

Jiaxuan Wang[1,2], Caroline J. Zinn[2], Maya Learmonth[1,2], Taylor D. Andrews[1,2], Zachary K. Snow[2], Laura Rae Elsbernd Becher[3], Allison P. Hershoff[3,6], Julieth A. Rincon Fajardo[3], Saranya Wyles[4], Christopher R. Paradise[3], Atta Behfar[5,6] ✉, Joy Wolfram[7,8,9] ✉, and LaTonya J. Hickson[2] ✉

[1] *Mayo Clinic Graduate School of Biomedical Sciences, Jacksonville, FL 32224, USA*
[2] *Division of Nephrology and Hypertension, Department of Medicine, Mayo Clinic Jacksonville, FL 32224, USA*
[3] *Rion, Inc., Rochester, MN 55902, USA*
[4] *Department of Dermatology, Mayo Clinic, Rochester, MN 55905, USA*
[5] *Department of Cardiovascular Diseases, Mayo Clinic, Rochester, MN 55905, USA*
[6] *Van Cleve Cardiac Regenerative Medicine Program, Mayo Clinic, Rochester, MN 55905, USA*
[7] *School of Chemical Engineering, The University of Queensland, Brisbane, QLD 4072, Australia*
[8] *Australian Institute for Bioengineering and Nanotechnology, The University of Queensland, Brisbane, QLD 4072, Australia*
[9] *Herston Biofabrication Institute, Metro North Health and The University of Queensland, Brisbane, QLD 4029, Australia*

Cite this article: *Nano Research*, **2026**, *19*, 94908496. https://doi.org/10.26599/NR.2026.94908496

ABSTRACT: Extracellular vesicle (EV)-based therapies are rapidly emerging as novel, regenerative cell-free strategies for treating diseases. A current good manufacturing practice (cGMP)-compliant, platelet-derived EV, known as purified exosome product (PEP), has been evaluated in several ongoing preclinical and clinical applications. PEP offers multiple advantages, including abundance and ambient temperature stability. Across 22 published studies, PEP demonstrated pro-angiogenic, anti-inflammatory, and pro-proliferative properties, yielding promising findings in wound, musculoskeletal, cardiovascular, and pulmonary conditions. PEP has been evaluated in phase 2 clinical trials for diabetic foot ulcers and phase 1 clinical trials for various wounds, osteoarthritis, and acute myocardial infarction. However, the therapeutic potential of PEP in kidney disease remains unexplored. Here, we summarize prior and ongoing PEP investigations and introduce PEP reparative effects in a murine model of diabetic kidney disease (DKD), the predominant cause of kidney failure globally. Preliminary findings reveal that intravenous PEP administration reduces kidney fibrosis and hyperglycemia in murine DKD and attenuates fibrogenesis in human proximal tubular cells *in vitro*. Collectively, PEP demonstrates robust capacity as a regenerative platform with promise to delay disease progression and restore health across multiple organ systems. Further large-scale investigations are warranted to support clinical translation of this promising EV-based technology.

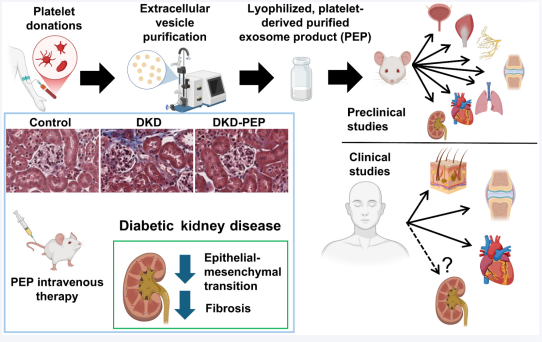

KEYWORDS: diabetes mellitus, fibrosis, exosomes, current good manufacturing practice, platelet, chronic kidney disease

1 Introduction

A platelet-derived extracellular vesicle (EV) product, purified exosome product (PEP), has demonstrated therapeutic potential across a range of conditions in both preclinical and clinical studies due to its pro-angiogenic, cytoprotective and anti-inflammatory properties. The first preclinical study applying this therapy was published in 2020 and the first clinical investigations began in 2021 [1, 2]. Several clinical trials have assessed PEP safety and early efficacy in acute myocardial infarction, osteoarthritis, split thickness skin grafts, radiation wounds, and diabetic foot ulcers [3–7]. PEP is manufactured by Rion Inc. (Rochester, Minnesota, United States) under current good manufacturing practice (cGMP) conditions.

Received: October 14, 2025; **Revised:** January 22, 2026
Accepted: January 28, 2026

✉Address correspondence to Atta Behfar, Behfar.Atta@mayo.edu; Joy Wolfram, j.wolfram@uq.edu.au; LaTonya J. Hickson, Hickson.LaTonya@mayo.edu

EVs are derived from apheresis-purified platelets obtained from blood collection centers licensed by the United States Food and Drug Administration (FDA) via a subtractive manufacturing process that yields intact, potent platelet EVs stabilized within a lyophilized powder cake [1, 8]. To minimize batch heterogeneity, each lot of PEP drug product is derived from a starting pool of multiple individual donors [9]. The final EV product is a lyophilized, off-white to light yellow powder, stored at room temperature and is shelf stable for up to two years. The final product can be readily reconstituted within the sterile vial at the point of care prior to administration [10]. This thermostable, off-the-shelf lyophilized product supports broad clinical distribution and practical application across diverse care settings. To date, clinical and experimental research applying PEP applications has involved a wide range of administration routes, including inhalation, topical application, and injections through intra-articular, intravenous, intramuscular, and intraperitoneal routes. Here, we provide a comprehensive overview of prior and ongoing investigations of PEP and, for the first time, demonstrate its therapeutic application via intravenous administration in a preclinical model of kidney disease, namely diabetic kidney disease (DKD), the most common cause of kidney failure globally [11, 12].

2 Experimental

2.1 Animal study

Eight-week-old male C57BL6/J mice were obtained from Jackson Laboratory (Bar Harbor, ME), and aged out to six months to approximate early adulthood in humans [13]. Mice were housed in plastic cages (maximum five per cage) in the animal facility under controlled conditions with a 12:12 h light–dark cycle with free access to water and food (standard mouse diet, Lab Diet 5053, St. Louis, MO, USA). To generate a DKD injury model, streptozotocin (STZ; Cayman Chemical Company) was administered via intraperitoneal injection (i.p.) at a dose of 50 mg/kg for five consecutive days (plus three additional days if target glucose was not met within two weeks). Blood glucose levels were measured after a six-hour fast using an Accu-Chek Guide glucometer and mice with fasting blood glucose > 250 mg/dL were considered diabetic. After 11 weeks of hyperglycemia, diabetic mice were randomly assigned to receive either vehicle (saline) or PEP (Rion, Rochester, MN) administered via tail vein injection over two consecutive days. Lyophilized PEP was reconstituted in sterile saline and adjusted to a final concentration of 4×10^{10} EVs/mL, with mice receiving 125 µL doses on two consecutive days. At the endpoint, 24-h urine collections were performed using metabolic cages. One to four weeks following vehicle/PEP administration, mice were euthanized by exsanguination under 3% isoflurane. Blood was drawn from the inferior vena cava and kidneys were harvested for subsequent analysis. Animal protocol (A00004821) was approved by the Mayo Clinic Institutional Animal Care and Use Committee and adhered to the National Institutes of Health Guide for the Care and Use of Laboratory Animals. PEP is manufactured by Rion Inc. (Rochester, Minnesota, USA) under current good manufacturing practice (cGMP) conditions. The PEP has been cleared by the U.S. Food and Drug Administration (FDA) for administration to human subjects in a Phase 2 clinical investigation (NCT06319287).

2.2 Cell culture experiments

In vitro studies were performed in human renal proximal tubule epithelial cells (PTEC; CellBiologics, Chicago IL) to examine PEP repair effects in the diabetic milieu. PTEC were maintained in complete media (H6621, CellBiologics, Chicago IL) supplemented with 10% fetal bovine serum (FBS) in a humidified atmosphere with 5% CO_2 at 37 °C. Experiments were performed at 60% confluence. PTEC were exposed to starvation media (complete media + 0.1% FBS) and then four days of incubation in control media, injury media, or prevention media. Control media consisted of complete media + 10% FBS. Injury media was composed of control media with high glucose (HG; 25 mM) and transforming growth factor-β (TGF-β) to mimic the diabetic microenvironment (R&D Systems, Minneapolis MN) at 5 ng/mL. Prevention media was comprised of HG plus TGF-β media with PEP at 5×10^9 EVs/mL.

2.3 Immunofluorescence

PTEC were stained in six-well plates using primary collagen IV (ab6586) and primary activin A (PA5-100101) respectively, and secondary antibody, goat anti-rabbit IgG (H+L) Alexa fluor 594 (A-11012). Antibodies were diluted 1:100 in 1% bovine serum albumin (BSA) + 3% Triton (Biovision, B2394-100). Cells were fixed for 20 min at room temperature, using 4% formaldehyde. Cells were washed twice using phosphate buffered saline (PBS) and permeabilized with 0.2% Triton in PBS for five minutes. Cells were then washed three times, then blocked with 5% BSA + 0.2% Triton in PBS for 30 min at room temperature. Primary antibody was added to cells and incubated overnight at 4 °C. After overnight incubation, cells were washed three times and incubated with secondary antibody protected from light for 30 min at room temperature. Cells were washed three times and counterstained with 4',6-diamidino-2-phenylindole (DAPI) (P36941). Imaging was performed using EVOS M5000 (Invitrogen, Waltham, MA, USA) and percent positive staining was calculated using ImageJ software by counting instances of positive stain and normalized to DAPI staining.

2.4 Reverse transcription quantitative real-time polymerase chain reaction (RT-qPCR)

Total RNA was isolated from kidney tissue (0.5–0.05 g) using PureLink RNA Mini Kit (Invitrogen, 12183018A, Waltham, MA) and cDNA was synthesized using SuperScript VILO Master Mix (Invitrogen, 11755050). Gene expression was analyzed by qPCR using Applied Biosystems QuantStudio Real-Time PCR software (Life Technologies, Carlsbad, CA). Fibrosis and epithelial-mesenchymal transition (EMT) markers were analyzed using TaqMan probes (Thermo Fisher Scientific, 4331182): FN1 (fibronectin 1, Homo sapiens: HS01549976_m1), COL1A1 (collagen type I alpha 1 chain, Homo sapiens: HS00164004_m1, Mus musculus: MM00801666_g1), COL4A1 (Homo sapiens: HS00266237_m, Mus musculus: MM01210125_m1) and INHBA (inhibin Subunit Beta A, Homo sapiens: HS01081598_m1, Mus musculus: MM00434339_m1, encoding Activin A) and Luna Universal qPCR Master Mix (New England Biolabs, M3004). EMT markers, including wingless-type MMTV integration site family member 5A (Wnt5a) and Vimentin, were analyzed using iTaq Universal SYBR Green Supermix (Bio-Rad, 1725122). Primer sequences were designed using the National

Center for Biotechnology Information Basic Local Alignment Search Tool (NCBI BLAST): *Wnt5a* (forward: 5'-CAACTGGCAGGACTTTCTCAA-3'; reverse: 5'-CATCTCCGATGCCGGAACT-3') and *Vimentin* (forward: 5'-CGTCCACACGCACCTACAG-3'; reverse: 5'-GGGGGATGAGGAAATAGAGGCT-3'). Gene expression was normalized to glyceraldehyde-3-phosphate dehydrogenase (GAPDH) or TATA-box binding protein (TBP). The $2^{-\Delta\Delta CT}$ method was used to calculate fold-change of gene expression.

2.5 Kidney histology

Mouse kidney tissue was fixed with 10% formalin, embedded in paraffin, and stained with Masson's trichrome and Picrosirius Red reagents to assess fibrosis. Random images were taken of the paraffin-embedded (5 μm) kidney tissue sections using Aperio AT2 Scanner and the Image Scope software. Analysis was performed by an operator blinded to the study groups, utilizing a fixed intensity threshold for the blue (Trichrome) and red (Picrosirius Red) channels to ensure objective and consistent pixel-wise quantification across all samples.

2.6 Cryogenic transmission electron microscopy (cryo-TEM)

Sample preparation: A vial of PEP was reconstituted in 1 mL of nanopure water and then diluted 1:2 in nanopure water. Albumin was removed using PureProteome Albumin Magnetic Beads (EMD Millipore Cat. SKMAGL19). After thorough mixing, 750 μL of beads were transferred to a 1.5 mL microcentrifuge tube, collected with a magnetic rack, and the buffer was discarded. The beads were washed twice with 750 μL of PBS, then 100 μL of PEP was added. The mixture was rotated at room temperature for one hour, the beads were collected on the side of the tube using the magnetic rack, and the albumin depleted fraction of PEP was transferred to a clean microcentrifuge tube.

Cryo-TEM method: Albumin-depleted fraction was diluted fourfold in water and preserved in vitrified ice on a holey carbon-coated TEM support grid. A 3 μL drop of the sample was applied to a cleaned grid, blotted with filter paper, and vitrified in liquid ethane. Grids were stored in liquid nitrogen until imaging with a Thermo Fisher Scientific Glacios Cryo-TEM at 200 kV, equipped with a Falcon direct electron detector. Vitreous ice grids were clipped into cartridges, transferred to a cassette, and loaded into the Glacios autoloader, all below −170 °C. Automated data collection was performed using Leginon software. High magnification images were taken at 73,000×. Images were acquired at a nominal under focus of −5.5 to −3.5 μm and electron doses of ~ 10^{-25} $e^-/Å^2$.

2.7 EV size/concentration measurement

PEP was analyzed via nanoparticle tracking analysis (NTA) using the NanoSight instrument (Malvern Panalytical). Control 100 nm polystyrene standard beads were diluted 1:1000 in water. The focus was adjusted to sharpen the edges of the beads while minimizing overexposure of the beads. The set focus was maintained through the remainder of sample analysis. The PEP sample was diluted 1:1000 in water prior to running on the NanoSight. The script in the NTA software was set to record three, thirty second videos of the particles in the flow cell with the syringe pump infusion rate set to 50. Analysis parameters were auto-set within the NTA software and results exported. Sample concentrations were multiplied by the dilution factor of 1000 for reporting.

2.8 Nano imager ONI (Oxford Nanoimaging, Inc.)

Sample preparation: one vial of PEP was resuspended in 1.0 mL of nanopure water and incubated at room temperature for two minutes. Complete resuspension of the powder cake was observed before EV detection.

EV capture and detection: EVs in the PEP sample were captured and detected using the EV Profiler 2 kit (Oxford Nanoimaging, Inc.) with phosphatidylserine capture and detection. The kit's CD81, CD63, and CD9 antibodies were used to detect surface markers. Following the manufacturer's instructions, all kit components, except the direct Stochastic Optical Reconstruction Microscopy (dSTORM) Imaging Buffer, were brought to room temperature. 10 μL of Surface Reagent was applied to the assay chip and incubated for 15 min. After washing with 100 μL of Wash Buffer, 10 μL of Capture Reagent was added and incubated for another 15 min. The chip was washed again, and 10 μL of the PEP solution with PS Capture Supplement was applied and incubated for 75 min at room temperature. Following another wash, 20 μL of Fixative was applied for 10 min, then washed off. 10 μL of staining buffer was applied and incubated for 10 min. The detection antibodies were diluted, and 10 μL was applied to the assay chip lanes, incubating for 50 min at room temperature, protected from light. After washing, 20 μL of Fixative was applied for 5 min, followed by another wash. dSTORM Imaging Buffer was prepared by combining 99 μL of Part A with 1 μL of Part B, mixed gently, and 20 μL of the prepared buffer was added to the assay chip lanes, which were then sealed. The assay chip was imaged on the Nanoimager, and images were analyzed using ONI CODI software.

2.9 Western blot

Capillary-based automated Western blot (Jess, ProteinSimple) of platelet (CD41) and EV markers (CD63, CD9, and Flotillin-1) were performed to determine the identity of PEP in control and test samples. First, the ExoEasy Maxi kit (QIAGEN Catalog #76064) was used according to the manufacturer's instructions to eliminate the non-EV proteins that are important for stabilizing PEP but interfere with antibody specificity in the Western blot assay. The protein content of the ExoEasy isolated EV-fractions were quantified via bicinchoninic acid (BCA) assay. Each EV-fraction was diluted to 1.0 mg/mL (protein loading for CD9 and Flotillin-1 (Flot-1)), 0.5 mg/mL (protein loading for CD63), and 0.02 mg/mL (protein loading for CD41), then combined with 5× fluorescent Master Mix (MM). Primary antibody anti-human CD9 (Cell Signaling Catalog #13403S) was used at 1:30; primary antibody anti-human Flot-1 (Abcam Catalog #AB133497) was used at 1:50; primary antibody anti-human CD63 (R&D Systems Catalog #MAB50482) was used at 100 μg/mL; primary antibody anti-human CD41 (Novus Catalog #NBP1-84581) was used at 1:30. The anti-rabbit detection module (ProteinSimple Catalog #DM-001) was used for the secondary antibody and chemiluminescent detection reagents with the 12–230 kDa Separation Module (ProteinSimple Catalog #SM-W004). The manufacturer's protocol was followed for plating and running the assay on the Jess instrument. Data was analyzed on Compass for Simple Western software (ProteinSimple).

2.10 PEP total protein measurement

Total protein content was evaluated via BCA assay using the Thermo Fisher Scientific BCA assay kit (Catalog #23227). PEP was diluted 1:50 in saline prior to testing. The samples, a saline

background control, and a BSA seven-point standard curve from 125–2000 mg/mL (Thermo Fisher Scientific Catalog #23208) were plated (25 mL/well) in technical triplicate. The BCA reagent was added (200 mL/well) and the plate was incubated at 37 °C for 30 min. The absorbance was measured at a wavelength of 562 nm using a Varioskan Lux (Thermo Scientific) spectrophotometer. To determine the protein concentration of the samples, absorbance values were compared to the linear fit standard curve generated from known concentrations of BSA. Sample concentration results were multiplied by the dilution factor of 50 for reporting.

2.11 Biochemical analysis

Blood glucose levels were determined after six hours of fasting using a handheld glucometer (Accu-Chek Aviva). In instances where glucose concentrations surpassed the system's measurable range, the upper limit of 601 mg/dL was recorded. Urine albumin levels were quantified via enzyme-linked immunosorbent assay (ELISA) using a commercial mouse albumin ELISA kit (Abcam, ab207620). Kidney function was evaluated by measuring plasma and urine creatinine concentrations using DetectX kits (KB02 and K002, respectively; Arbor Assays). For samples yielding concentrations outside the detectable range of the standard curve, values were assigned the limit of the highest or lowest standard point, as appropriate.

2.12 Geolocation information

This study was performed collaboratively between Mayo Clinic campuses in Jacksonville, FL, USA, and Rochester, MN, USA, with additional contributions from The University of Queensland, Australia.

3 Results

3.1 PEP characterization and manufacturing process

Comprehensive characterization of PEP is provided in Fig. 1. Cryo-TEM confirms the expected, spherical morphology and diameter of the vesicles with intact lipid bilayers, a key authentication feature (Fig. 1(a)) [14]. NTA was used to determine the size distribution and concentration of PEP, revealing a mode particle size of 130.1 ± 12.2 nm and a concentration of $5.11 \times 10^{11} \pm 3.03 \times 10^{10}$ EVs/mL (Fig. 1(b)). Single-vesicle phenotyping via dSTORM shows the presence of exosomal markers CD81, CD63, and CD9 on individual vesicles (Fig. 1(c)), and the expression of these markers, along with the platelet-origin marker CD41, was confirmed by Western blot (Fig. 1(d)). The final product has a total protein concentration of approximately 60 mg/mL (Fig. 1(e)) and is manufactured as a stable, lyophilized powder, as illustrated in the process schematic (Fig. 1(f)).

3.2 Preclinical and clinical studies applying PEP

To date, a variety of studies demonstrated therapeutic effects of PEP in preclinical and clinical studies, as summarized in Table 1. PEP has been applied in a variety of organ systems, including skin, spinal cord, vagina, bladder/urethra, muscle/tendons/joints, nerves, lungs, and heart [8–10, 15–24]. Currently, early phase (1 and 2) clinical trials examine PEP safety and early efficacy signals for treatment of acute myocardial infarction, osteoarthritis, radiation wounds, skin graft wounds, and diabetic foot ulcers [3–7]. PEP has been delivered through multiple administration routes, including topical (most common), intracoronary, intra-articular, intramuscular, nebulization, intraperitoneal, intravenous through the femoral vein sheath, injected on a mesh, and injected directly on the area of interest during procedures, broadening its application range [8, 9, 15, 22–26]. Delivery has been facilitated using collagen, hyaluronic acid, and fibrin hydrogels or scaffolds to direct therapy and enhance PEP localized retention. To further examine biodistribution of PEP, a pulmonary biodistribution study was conducted in pigs. Rizzo et al. found that PEP uptake primarily localized to the lung parenchyma after intravenous, pulmonary artery balloon catheter-guided, and nebulization delivery routes [26]. Interestingly, 15 min after PEP treatment, no uptake was observed in the liver, heart, spleen, or kidney by an *in vivo* imaging system (IVIS) with either delivery approach. Collectively, these discussed studies assessed PEP repair effects in multiple organs and diseases. However, PEP reparative effects in the kidney are unknown.

3.3 PEP reduces fibrosis-associated markers in human kidney tubule cells *in vitro*

We hypothesized that PEP would have therapeutic effects in the diabetic kidney and kidney cells exposed to the diabetic milieu. High glucose plus TGF-β (HG-TGF-β) exposure increased protein expression of fibrosis marker type IV collagen and pro-fibrosis and senescence marker activin A in human proximal tubule epithelial cells (PTECs) (Fig. 2). Representative images of these changes are shown on morphologic examination and immunofluorescence staining for collagen type IV and activin A (Fig. 2(a)). PEP administration at time of injury led to decreased mRNA expression of type IV collagen, fibronectin, and activin A expression compared to HG-TGF-β controls (Fig. 2(b)). Non-significant trends were found for a reduction in type I collagen.

3.4 Intravenous delivery of PEP in a murine model of DKD reduces fibrosis markers

We then examined the effects of intravenous delivery of PEP in a murine model of DKD (Fig. 3(a)). STZ-induced diabetes mellitus is a type I diabetes model, in which STZ damages pancreatic β-cells and impairs insulin production leading to hyperglycemia. After several weeks of hyperglycemia, STZ mice had reduced body weight, heart weight, and kidney/body weight ratios (Table 2), but increased urine volume as expected in the context of hyperglycemia (Fig. 3(b)). By four weeks post-injection, PEP-treated STZ mice showed significant improvements in physiological parameters, including less body weight loss and improved kidney/body weight ratio vs STZ controls. Surprisingly, lower blood glucose levels were also observed, potentially indicating improved pancreatic function. Non-significant trends were found for a reduction in urine volume (likely due to less hyperglycemia) versus STZ controls. Plasma creatinine was higher in STZ mice (versus controls) and trended (non-significant) lower in PEP-treated mice (versus STZ). STZ mice demonstrated albuminuria (urine albumin/creatinine ratio) but no differences were found after PEP.

Given that kidney fibrosis is the common final endpoint for disease, studies were performed to examine PEP repair on pro-fibrosis and EMT markers. As anticipated, STZ mice had increased markers of kidney fibrosis. Representative images of trichrome and picrosirius red staining are shown (Fig. 3(c)). At one-week post-

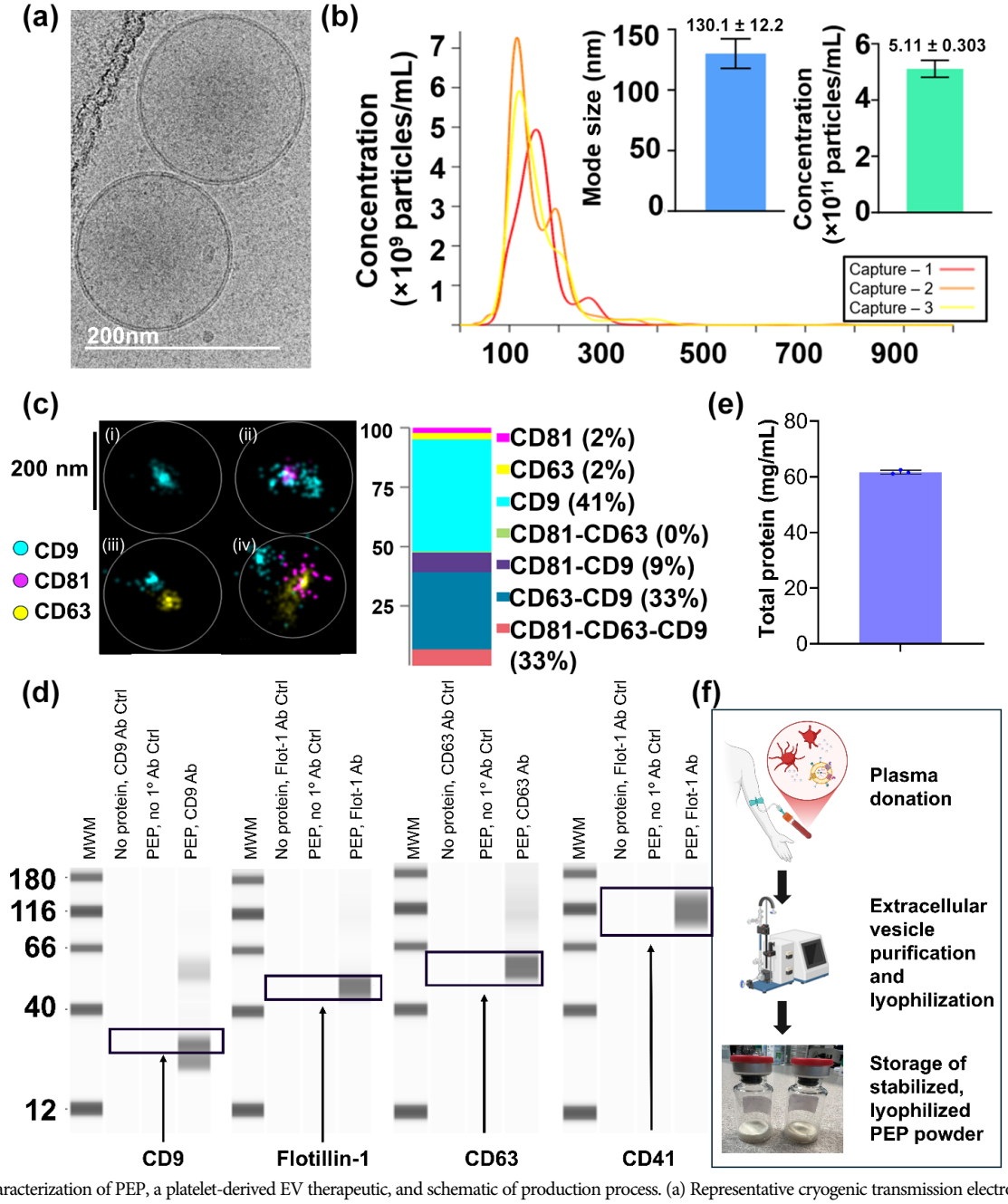

Figure 1 Characterization of PEP, a platelet-derived EV therapeutic, and schematic of production process. (a) Representative cryogenic transmission electron microscope images of EV morphology (lipid bilayers are visible). (b) Size distribution, mode size, and concentration assessed by nanoparticle tracking analysis. (c) Surface marker profile of PEP assessed by super-resolution microscopy. Diameter of circle with representative images: (i) CD9 single-positive EV, (ii) CD81-CD9 double-positive EV, (iii) CD63-CD9 double-positive EV, and (iv) CD9-CD81-CD63 triple-positive EV. Scale bar: 200 nm. (d) Western blot of EV and platelet markers: CD9, flotillin-1, CD63, and CD41. (e) Protein concentration determined by a bicinchoninic acid assay. (f) Schematic illustrating the PEP manufacturing pipeline involving donor-apheresis for platelets, culture, EV isolation, lyophilization, and product presentation. Ab: antibody; MWM: molecular weight marker.

PEP injection, pro-fibrosis markers, including trichrome and picrosirius red staining were lower than STZ controls. Additionally, one week after PEP, mRNA expressions of type I collagen and Wnt5a were lower than STZ groups (Fig. 3(d)). Interestingly, STZ did not change vimentin mRNA expression versus controls, an EMT marker and mediator of wound healing and regenerative processes, but PEP mice had higher expression (versus STZ and controls) [27]. Non-significant trends were found for a reduction in type IV collagen and activin A (vs STZ) at four weeks following PEP administration.

4 Discussion

Our studies demonstrate, for the first time, the therapeutic potential of PEP in a kidney disease model. Moreover, systemic administration via tail vein injection had impact locally on the diabetic kidney and led to marked reduction in fibrosis-related kidney markers in addition to improvement in physiological parameters, including hyperglycemia. As a final common endpoint, fibrosis and excessive deposition of extracellular matrix proteins, leads to progressive loss of kidney function. Our findings show that PEP treatment significantly reduced collagen deposition. These

Table 1 Summary of clinical and preclinical studies using PEP manufactured by Rion Inc.[a]

Rion PEP preclinical and clinical investigations			
Type	Condition	Administration route	Ref.
		Clinical studies	
Case study	Chemoradiation-induced scalp wounds	Topical (in Bellafill dermal filler and Tisseel fibrin sealant)	Pumford et al., 2024 [25]
Phase I	Acute myocardial infarction (RioCard001)	Intracoronary infusion	NCT04327635 [3]
Phase I	Knee Osteoarthritis (RioMSK001)	Intra-articular injection (alone or in Euflexxa hyaluronic acid gel)	NCT06463132 [5]
Phase I	Skin graft donor site wound	Topical (alone or in Tisseel fibrin sealant)	NCT04664738 [4]
Phase I	Chronic radiation ulcer	Topical (in Tisseel fibrin sealant)	NCT06793748 [6]
Phase II	Diabetic foot ulcers (RioDerm001)	Topical (in Tisseel fibrin sealant)	NCT06319287 [7]
		Preclinical studies	
Porcine	Biodistribution	Intravenous, pulmonary artery balloon catheter, or nebulization	Rizzo et al., 2024 [26]
Porcine	Stress urinary incontinence	At repair site (in collagen-1 hydrogel or Tisseel fibrin sealant)	Rolland et al., 2022 [8]
Porcine	Vaginal mesh exposure	Fibromuscular tissue under mesh exposure site (in type I bovine collagen)	Kisby et al., 2021 [15, 16]
Canine (*ex vivo*)	Tendon injury	At repair site (in Tisseel fibrin sealant)	Shi et al., 2021 [20]
Rat	T9-T10 laminectomy + contusion of spinal cord	Intrathecal, intravenous	Zamanian et al., 2023 [24]
Rat	Volumetric muscle loss	At repair site (in Tisseel fibrin sealant)	Mazzucchelli et al., 2023 [22]
Rat	Sciatic nerve defect	On decellularized nerve allograft (in Tisseel fibrin sealant)	Wang et al., 2023 [21]
Rat	Sciatic nerve defect	On nerve autograft (in Tisseel fibrin sealant)	Ikumi et al., 2021 [10]
Rat	Rotator cuff tear	At repair site (in Tisseel fibrin sealant)	Ren et al., 2021 [17]
Rabbit	Achilles tenotomy	At repair site (in type 1 collagen scaffold)	Wellings et al., 2021 [19]
Rabbit	Wound healing	At repair site (inTisseel fibrin sealant)	Shi et al., 2021 [18]
Mouse	Emphysema	Nebulization	Xuan et al., 2024 [23]
Mouse	Viral myocarditis	Intraperitoneal	Beetler et al., 2023 [9] 2025[61]
Cell culture (3D)	Decellularized nerve allografts	n/a	Rademakers et al., 2024 [30]
Cell culture	Dorsal root ganglion neurite outgrowth assay	n/a	Saffari et al., 2023 [31]
Cell culture	Patient chondrocytes derived from osteoarthritis	n/a	Shi et al., 2023 [32]
Cell culture	Human endometrial cells (wound healing)	n/a	Miller et al., 2022 [29]
Cell culture	Canine tenocytes	n/a	Qi et al., 2020 [1]

[a]This table compiles published and ongoing studies investigating the therapeutic applications of PEP. Studies are organized by type (clinical and preclinical), target condition, and route of administration. Clinical applications span cardiovascular, musculoskeletal, and wound healing indications, ranging from case studies to phase II clinical trials. Preclinical studies include various animal models with diverse delivery routes, including topical application in hydrogels or scaffolds, intravascular or skeletomuscular administration, and nebulization. *In vitro* studies involve relevant patient-derived or species-specific cell types. Clinical trials are listed with ClinicalTrials.gov identifiers: NCT04327635, NCT06463132, NCT06793748, NCT04664738, and NCT06319287. n/a: not applicable.

therapeutic PEP findings were supported by *in vitro* studies in human kidney tubule cells exposed to the diabetic milieu. These early findings suggest that PEP possesses kidney-repair effects and can be further examined across other kidney diseases.

As summarized earlier, PEP is also currently being assessed in clinical trials and has demonstrated advantageous response in preclinical studies across a broad range of non-kidney applications. Notably, PEP's formulation offers practical advantages, including room temperature stability for up to two years, which substantially reduces logistical burdens compared to other cell-derived products [28]. The versatility of PEP is demonstrated by multiple disease context and administration routes, as in Table 1, including topical applications in skin wounds, diabetic foot ulcers, intracoronary infusion in acute myocardial infarction, and intra-articular injections for osteoarthritis. In parallel with clinical studies, preclinical development also continues across a broad range of applications. While ongoing clinical trials highlight the strong potential of PEP for skin, wound and skeletomuscular regeneration, our data on PEP in treating DKD, along with recent myocarditis and nerve defect recovery, collectively demonstrate the broader therapeutic potential of PEP for visceral applications beyond skin and muscle regeneration [9, 21]. *In vitro* studies also have shown that PEP promotes neurite growth, stimulates proliferation and wound healing in human endometrial cells, and enhances proliferation and migration while reducing apoptosis in osteoarthritis patient-derived chondrocytes, thereby supporting pro-chondrogenic activity [29–32]. The wide-ranging applicability of PEP across both clinical and non-clinical settings highlights a strong

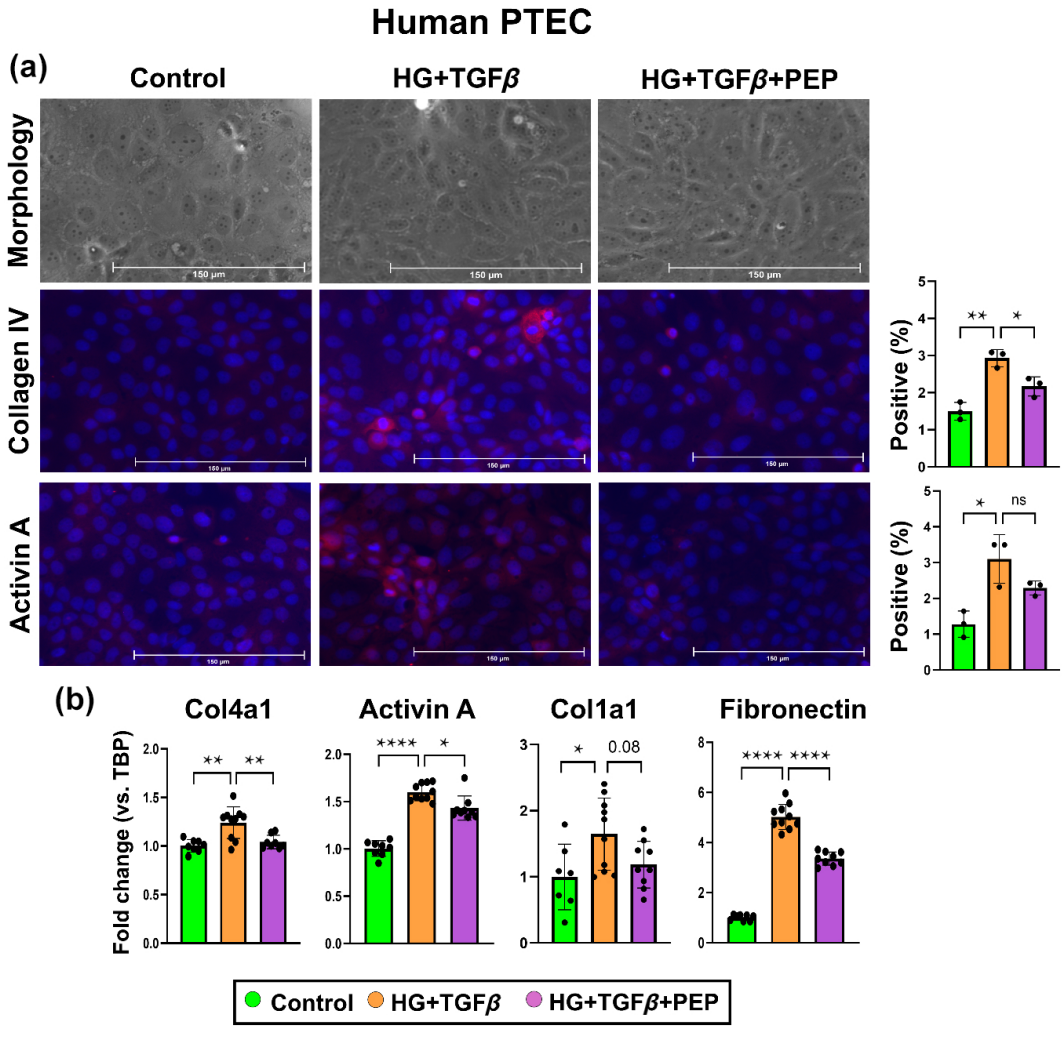

Figure 2 PEP reduces fibrosis-associated markers in human kidney tubule cells *in vitro*. PTEC were serum-starved for 24 h, then treated with HG (25 mM) plus TGF-*β* (5 ng/mL) to mimic the diabetic microenvironment. Media was then supplemented with PEP (5×10^9 EVs/mL) or without (control) for four days. (a) Representative images of light microscopy and immunofluorescence staining for collagen IV and activin A in control, HG+TGF-*β*, and HG+TGF-*β*+PEP groups. (b) RT-qPCR analysis of type I collagen (col1a1), type IV collagen (col4a1), fibronectin, and activin A mRNA expression levels. All data are presented as mean ± standard deviation (SD). Statistical significance: $^*P < 0.05$; $^{**}P < 0.01$; $^{***}P < 0.005$; $^{****}P < 0.001$. Outliers were determined by GraphPad ROUT method (Robust regression and Outlier removal method) (maximum false discovery rate = 1%). Data was analyzed using Brown-Forsythe and Welch ANOVA test. Control: PTECs treated with starvation followed by complete medium; HG+TGF-*β*: PTECs treated with starvation followed by high glucose and TGF-*β*; PEP: PTECs treated with starvation followed by high glucose, TGF-*β*, and PEP. TBP: TATA-box binding protein.

Table 2 Comparisons of key physiological parameters at endpoint following PEP treatment in a murine model of DKD[a]

	Endpoint body weight (g)	Left kidney weight (g)	Right kidney weight (g)	Heart weight (g)	Left kidney/body weight ratio (g/g)	Right kidney/ body weight ratio (g/g)
Control	31.51 ± 3.60	0.27 ± 0.04	0.27 ± 0.05	0.19 ± 0.02	0.009 ± 0.002	0.009 ± 0.002
STZ	24.87 ± 2.44 **	0.27 ± 0.03	0.28 ± 0.04	0.15 ± 0.03 **	0.011 ± 0.002 **	0.011 ± 0.002 **
STZ-PEP	28.82 ± 3.39 *	0.24 ± 0.03	0.27 ± 0.04	0.17 ± 0.02	0.008 ± 0.002 *	0.009 ± 0.002, $P = 0.1$

[a]Physiological parameters measured four weeks post-injection include body weight, blood glucose levels, individual organ weights, and 24-h urine volume. Data are presented as mean ± standard deviation. Statistical comparisons were performed using Kruskal-Wallis one-way ANOVA across control, STZ, and STZ-PEP groups. * indicates a significant difference between STZ and STZ-PEP; ** indicates a significant difference between STZ and control. Significance: $P < 0.05$.

translational potential in addressing diverse tissue repair and inflammatory conditions.

Importantly, we found that systemic (or intravenous) administration in rodents offers therapeutic benefits in the kidneys and potentially indirect evidence in the pancreas (hyperglycemia). Intravenous administration provides the advantage of being clinically feasible with low procedural risk and readily implementable. While the biodistribution and kidney localization of PEP remain insufficiently characterized in both murine models and humans, their biological trafficking is influenced by multiple factors including lipid compositions, surface proteins, glycan profiles, and their interactions with tissue-specific receptors and the immune

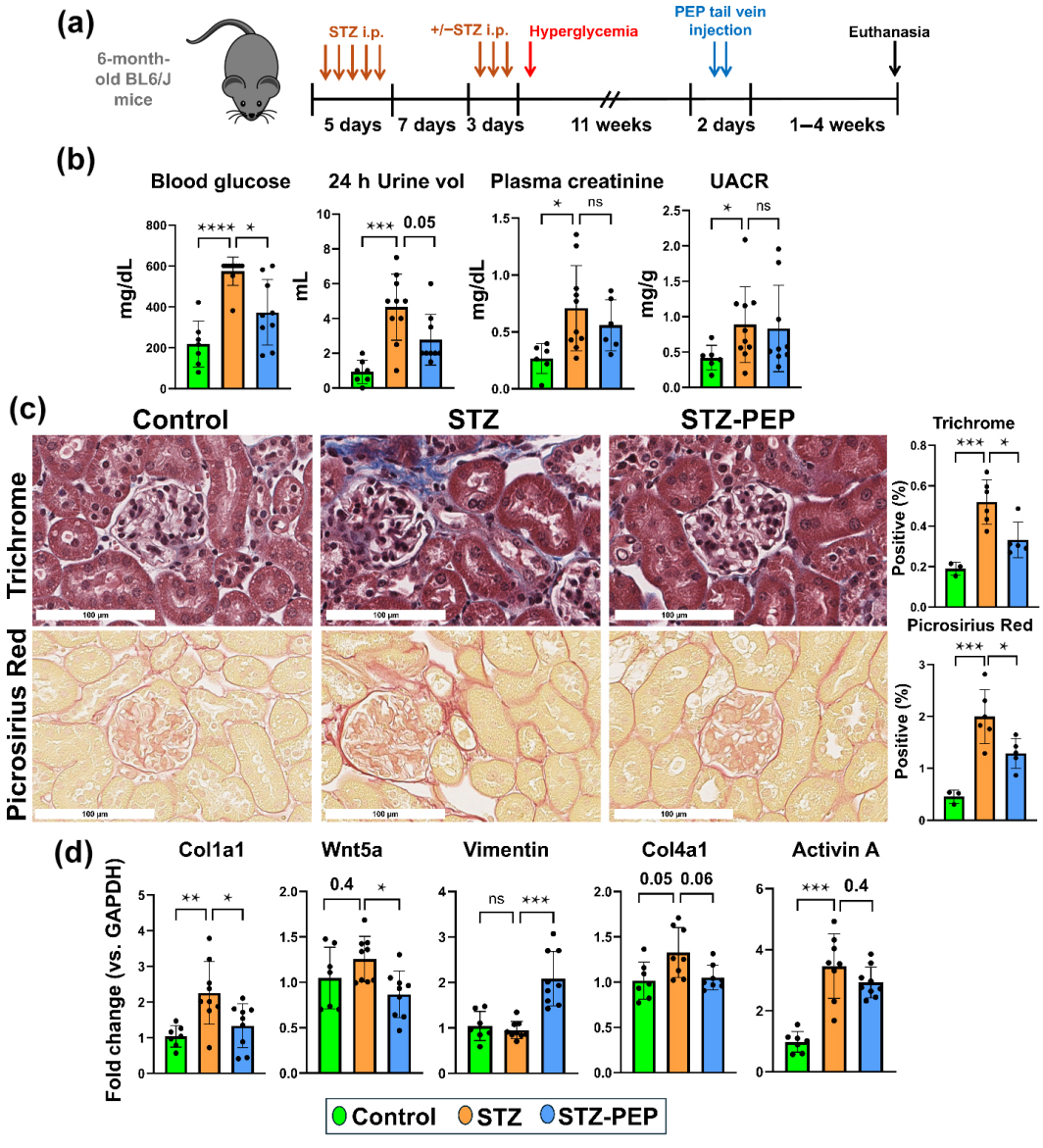

Figure 3 PEP reduces kidney fibrosis in murine diabetic kidney disease. (a) Schematic of STZ-induced diabetic mice treated with PEP injection over two days at 11 weeks after hyperglycemia. Mice were euthanized and tissue was harvested after one and four weeks. (b) Four weeks post-PEP administration, 24-h urine volume was recorded, and blood glucose, plasma creatinine, and albuminuria were determined by Accu-Chek Aviva glucometer and ELISA. In instances where glucose concentrations surpassed Accu-Chek Aviva glucometer measurable range, the upper limit of 601 mg/dL was recorded. (c) Representative images (scale bars: 100 μm) of Masson's Trichrome and Picrosirius Red staining of paraffin-embedded kidney sections from control, STZ-treated, and STZ+PEP-treated mice. Quantification of fibrosis was determined by trichrome (% blue area) and Picrosirius Red staining (% red area), showing a statistically significant reduction in fibrosis in the STZ+PEP group. (d) One week and four weeks post-PEP administration, RT-qPCR analysis was performed on kidney tissue for collagen I, Wnt5a, and vimentin (one week), as well as collagen IV and activin A (four weeks). All data are presented as mean ± SD. Outliers were determined by ROUT test (maximum false discovery rate = 1%). Statistical significance: $^{*}P < 0.05$; $^{**}P < 0.01$; $^{***}P < 0.005$; $^{****}P < 0.001$. Data was analyzed using Brown-Forsythe and Welch ANOVA test. Control: saline for disease induction and therapeutic administration; STZ: streptozotocin for disease induction and saline for therapeutic administration; STZ+PEP: streptozotocin for disease induction and PEP for therapeutic administration. UACR, urine albumin creatinine ratio; Urine Vol, urine volume.

system [33, 34]. Systemically administered nanoparticles, including EVs, face rapid clearance by the mononuclear phagocyte system following opsonization by the biomolecular corona, a process that triggers immune cell engulfment [35–37]. To overcome these barriers and improve the efficacy of EV-based therapies for DKD, various engineering techniques have been developed. Kidney injury molecule-1 (KIM-1) antibody–mediated targeting has been shown to enhance EV accumulation and therapeutic efficacy in injured kidneys [38]. Similarly, EVs derived from human umbilical cord mesenchymal stem cells (MSC)-EVs engineered to overexpress alkylation B homolog 5 (ALKBH5), exhibit significantly enhanced therapeutic efficacy in DKD models compared to unmodified MSC-EVs [39]. Recently, ILIAS Biologics Inc. received approval in Australia to initiate a first-in-human clinical trial evaluating ILB-202 in the treatment of cardiac surgery-associated acute kidney injury [40]. ILB-202 is an engineered, allogeneic EV derived from HEK293 cells and loaded with a super-repressor IκBα which inhibits nuclear factor kappa-light-chain-enhancer of activated B cells (NF-κB) translocation into the nucleus, hence attenuating inflammatory responses [41]. Alternative delivery approaches, such

as hydrogel-based formulations enabling direct-to-kidney parenchymal administration, may also enhance localized retention and further potentiate their therapeutic efficacy [42].

A growing pipeline of preclinical and clinical products continues to be developed. MSC-EVs show great therapeutic promise, especially in tissue repair and immune modulation, but their broader clinical translation is limited by manufacturing challenges. We and others have demonstrated MSC kidney repair effects in patients with DKD and chronic kidney disease [43–46]. We recently began administering MSCs to individuals with kidney disease through a United States FDA authorized compassionate use program [47]. Few clinical trials applying EVs in kidney disease have been reported. For example, Nasser et al. examined the effects of umbilical cord MSC-EVs in patients with chronic kidney disease [48]. In this study, patients received MSC-EVs both through intravenous/systemic and intra-arterial routes to the renal arteries with findings of improved kidney function from baseline to 12 weeks versus controls. Systemically-administered EV-based clinical trials for kidney disease have been slow to advance. Unfortunately, MSCs have a finite expansion capacity and require complex, costly culture systems, making even large-scale bioreactor approaches challenging in terms of scalability [49]. In contrast, biofluid-derived products, such as PEP, can be obtained in much higher yields in shorter time frames, circumventing MSC-EVs production bottlenecks [50]. Other early phase clinical trials are examining the therapeutic effects of PEP and EV technology [51, 52]. By leveraging a readily available, scalable source, PEP addresses key manufacturing and therapeutic limitations of MSC-EVs while offering broad applications such as a topically applied platelet-derived exosome product for dermatologic conditions [53–55] to PEP for heart disease to osteoarthritis.

In our preliminary kidney-focused studies, significant kidney function recovery shown by plasma creatinine and kidney injury (albuminuria) was not observed within this timeframe and PEP dose. However, a collective improvement in murine health was evident following PEP administration. This improvement was demonstrated by a consistent reduction in mRNA expression of fibrotic markers, decreased collagen deposition in the kidney, and improvement of physiological parameters including body weight, kidney weight, blood glucose (pancreas function), and urine volume. Given that this preliminary study applied a single-dose regimen, it is likely that higher PEP dosages or repeat dosing protocols may yield more pronounced therapeutic outcomes in the treatment of DKD.

While our preliminary findings in a murine DKD model are encouraging, some limitations should be acknowledged. First, this study was restricted to a single disease model, which may not capture the full spectrum of DKD pathophysiology, in particular the effects of insulin resistance. The STZ model primarily reflects type 1 diabetes, whereas type 2 diabetes is most common worldwide. Nonetheless, the effects on hyperglycemia-induced kidney injury were robust and likely allow for generalizability of our findings. Future large-scale PEP investigations will benefit from incorporation of type 2 diabetes models. Additionally, incorporation of first-line clinical drugs, as comparator groups or in combination with PEP, may allow for comparison between treatment groups in addition to assessment of synergistic therapeutic effects. Second, these preliminary studies only examined markers of kidney fibrosis and EMT. DKD is a complex, multifactorial disease with altered immune cell profiles and other pathogenic changes [42, 56]. Future studies examining additional endpoints, including inflammation, cellular senescence, and mitochondrial injury, may provide broader insights to understanding PEP mechanisms of kidney repair. Moreover, additional studies assessing the improvements in glucose levels after PEP can be further examined. Third, the underlying therapeutic mechanisms of EV-based therapies remain underexplored with key challenges including an incomplete understanding of anti-fibrotic and pro-repair mechanisms of action and active cargo responsible for therapeutic effects. Dedicated studies of EV biomolecules, which drive these therapeutic effects, should be further explored. Fourth, our study demonstrates repair effects of PEP at 1–4 weeks. This timeframe is consistent with other investigations applying MSC and MSC-EVs in murine kidney disease models [57–60], as well as the non-topical application of PEP in other murine contexts [9, 24, 61]. However, extended follow-up periods may provide insights into longer term effects of PEP therapy. Moreover, repeat dosing will likely be necessary to maintain these effects long-term in the kidney. Addressing these gaps in future studies will be essential for advancing PEP toward clinical application in DKD and other kidney diseases.

5 Conclusions

Several decades of preclinical and clinical research investigating the therapeutic utility of stem cell and stem cell-derived regenerative therapeutics has resulted in significant advances in regenerative medicine. However, cell-based therapies present substantial challenges when considering scalability and democratization. As a result of the increased focus on cell-based therapies, a better understanding of how cells exert their therapeutic effect has led to a new appreciation for the importance of the cell secretome and therapeutic utility of EVs. Now, EVs are gaining attention as a standalone novel class of regenerative therapeutics that present several advantages over cell-based approaches. In an effort to realize the therapeutic potential of EV-based therapeutics and overcome the limitations of cell-based therapies, Rion Inc., a biotechnology company spun out of the Mayo Clinic, has remained focused on the production of clinical-grade EVs at scale to enable translation to clinical practice. In the work presented here, we highlight PEP, a clinical-grade EV product derived from platelets and produced under cGMP conditions. The therapeutic potential and safety of PEP are currently being evaluated across several clinical trials. Our preliminary preclinical investigation demonstrates that PEP mitigates kidney fibrosis and reduces hyperglycemia in a mouse model of DKD suggesting need for additional studies. These data, when considered along with prior research in other applications, suggest a broad therapeutic potential of PEP. Continued preclinical validation and expanded clinical testing are essential to determine PEP's full applicability for disease management.

Data availability

The data supporting the findings of this study are available from the corresponding author upon reasonable request.

Acknowledgements

This research was supported by National Institutes of Health (NIH: Nos. AG076537 (L. J. H. and J. W.); DK101405, DK118120, DK07013, DK123492 (L. J. H.), DK109134 (L. J. H.)); and Mayo Clinic Florida Center for Regenerative Biotherapeutics.

Declaration of competing interest

L. J. H. serves as a consultant for Resolution Therapeutics and ETTA Biotechnology. J. Wo. has been a board member or scientific advisor of biomedical companies: Omnidermal, Genomill, and Pharmatest Services. Ionis Pharmaceuticals, Sartorius, and Sanofi have sponsored or are sponsoring research in JWo's laboratory. Rion Inc. supplied the clinical-grade EV material evaluated in the study. S. W. is a consultant for Rion Aesthetics. L. R. E. B., A. H., J. A. R. F., and C. P. are employees of Rion Inc. A. B. is CEO and co-founder of Rion Inc. This research has been reviewed by the Mayo Clinic Conflict of Interest Review Board and was conducted in compliance with Mayo Clinic Conflict of Interest policies. No conflicts of interest, financial or otherwise, are declared by the other authors.

Author contribution statement

J. Wa.: Data curation, formal analysis, visualization, writing – orginal draft (Lead), writing – review & editing (Lead). C. J. Z.: Data curation, formal analysis, visualization, writing – original draft, writing – review & editing. M. L.: Data curation, visualization, writing – review & editing. T. D. A.: Data curation, visualization, writing – review & editing. Z. K. S.: Data curation, visualization, writing – review & editing. L. R. E. B.: Data curation, visualization, writing – review & editing. A. P. H.: Data curation, visualization, writing – review & editing. J. A. R. F.: Data curation, visualization, writing – review & editing. S. W.: Visualization, writing – review & editing. C. R. P.: Resources, validation, writing – review & editing. A. B.: Resources, visualization, writing – review & editing. J. Wo.: Conceptualization, funding acquisition, Supervision (Lead), visualization, writing – original draft (Lead), writing – review & editing. L. J. H.: Conceptualization, formal analysis, funding acquisition, investigation, methodology, project administration (Lead), resources (Lead), supervision (Lead), validation, visualization, writing – original draft (Lead), writing – review & editing (Lead).

Informed consent

Not applicable.

Ethics statement

The animal experiments were carried out following the guidelines of Mayo Clinic Institutional Animal Care and Use Committee and adhered to the National Institutes of Health Guide for the Care and Use of Laboratory Animals. Animal studies were approved by the Mayo Clinic institutional animal care and use committee (IACUC) under protocol A00004821.

Use of AI statement

None.

References

[1] Qi, J.; Liu, Q.; Reisdorf, R. L.; Boroumand, S.; Behfar, A.; Moran, S. L.; Amadio, P. C.; Gingery, A.; Zhao, C. F. Characterization of a purified exosome product and its effects on canine flexor tenocyte biology. *J. Orthop. Res.* **2020**, *38*, 1845–1855.

[2] Behfar, A.; Terzic, A. *Pipeline* [Online]. Rion therapeutics: Rion therapeutics, 2025. https://riontx.com/pipeline/ (accessed Jan 24, 2025).

[3] Mayo Clinic. *Safety Evaluation of Intracoronary Infusion of Extracellular Vesicles in Patients Following Coronary Stent Implantation* [Online]. 2021. https://clinicaltrials.gov/study/NCT04327635 (accessed Jan 12, 2026).

[4] Rion Inc. *PEP on a Skin Graft Donor Site Wound* [Online]. 2021. https://clinicaltrials.gov/study/NCT04664738 (accessed Jan 1, 2026).

[5] Rion Inc. *Phase 1b Clinical Trial to Evaluate PEP and EUFLEXXA for Knee Osteoarthritis (KOA)* [Online]. 2024. https://clinicaltrials.gov/study/NCT06463132 (accessed Jan 1, 2026).

[6] Rion Inc. *Study to Evaluate the Safety, Tolerability, and Efficacy of PEP-TISSEEL in Subjects with Chronic Radiation Ulcer* [Online]. 2025. https://clinicaltrials.gov/study/NCT06793748 (accessed Jan 1, 2026).

[7] Rion Inc. *Phase 2a Multi-Center Prospective, Randomized Trial to Evaluate the Safety & Efficacy of Topical PEP-TISSEEL for Diabetic Foot Ulcers (DFU)* [Online]. 2026. https://clinicaltrials.gov/study/NCT06319287 (accessed Jan 1, 2026).

[8] Rolland, T. J.; Peterson, T. E.; Singh, R. D.; Rizzo, S. A.; Boroumand, S.; Shi, A.; Witt, T. A.; Nagel, M.; Kisby, C. K.; Park, S. et al. Exosome biopotentiated hydrogel restores damaged skeletal muscle in a porcine model of stress urinary incontinence. *npj Regen. Med.* **2022**, *7*, 58.

[9] Beetler, D. J.; Bruno, K. A.; Watkins, M. M.; Xu, V.; Chekuri, I.; Giresi, P.; Di Florio, D. N.; Whelan, E. R.; Edenfield, B. H.; Walker, S. A. et al. Reconstituted extracellular vesicles from human platelets decrease viral myocarditis in mice. *Small* **2023**, *19*, 2303317.

[10] Ikumi, A.; Gingery, A.; Toyoshima, Y.; Zhao, C. F.; Moran, S. L.; Livia, C.; Rolland, T.; Peterson, T.; Sabbah, M. S.; Boroumand, S. et al. Administration of purified exosome product in a rat sciatic serve reverse autograft model. *Plast. Reconstr. Surg.* **2021**, *148*, 200e–211e.

[11] Kidney Disease: Improving Global Outcomes (KDIGO) Diabetes Work Group. KDIGO 2022 clinical practice guideline for diabetes management in chronic kidney disease. *Kidney Int.* **2022**, *102*, S1–S127.

[12] IDF. *Diabetes Atlas, 11th Edition 2025* [Online]. 2025. https://diabetesatlas.org/media/uploads/sites/3/2025/04/IDF_Atlas_11th_Edition_2025-1.pdf (accessed Jul 2, 2025).

[13] Dutta, S.; Sengupta, P. Men and mice: Relating their ages. *Life Sci.* **2016**, *152*, 244–248.

[14] Broad, K.; Walker, S. A.; Davidovich, I.; Witwer, K.; Talmon, Y.; Wolfram, J. Unraveling multilayered extracellular vesicles: Speculation on cause. *J. Extracell. Vesicles* **2023**, *12*, e12309.

[15] Kisby, C. K.; Shadrin, I. Y.; Peng, L. T.; Stalboerger, P. G.; Trabuco, E. C.; Behfar, A.; Occhino, J. A. Impact of repeat dosing and mesh exposure chronicity on exosome-induced vaginal tissue regeneration in a porcine mesh exposure model. *Female Pelvic Med. Reconstr. Surg.* **2021**, *27*, 195–201.

[16] Kisby, C. K.; Shadrin, I. Y.; Rolland, T. J.; Stalboerger, P. G.; Zhou, B. R.; Trabuco, E. C.; Behfar, A.; Occhino, J. A. Exosome-induced vaginal tissue regeneration in a porcine mesh exposure model. *Female Pelvic Med. Reconstr. Surg.* **2021**, *27*, 609–615.

[17] Ren, Y.; Zhang, S. W.; Wang, Y. C.; Jacobson, D. S.; Reisdorf, R. L.; Kuroiwa, T.; Behfar, A.; Moran, S. L.; Steinmann, S. P.; Zhao, C. F. Effects of purified exosome product on rotator cuff tendon-bone healing *in vitro* and *in vivo*. *Biomaterials* **2021**, *276*, 121019.

[18] Shi, A.; Li, J. L.; Qiu, X. Y.; Sabbah, M.; Boroumand, S.; Huang, T. C. T.; Zhao, C. F.; Terzic, A.; Behfar, A.; Moran, S. L. TGF-β loaded exosome enhances ischemic wound healing *in vitro* and *in vivo*. *Theranostics* **2021**, *11*, 6616–6631.

[19] Wellings, E. P.; Huang, T. C. T.; Li, J. L.; Peterson, T. E.; Hooke, A. W.; Rosenbaum, A.; Zhao, C. D.; Behfar, A.; Moran, S. L.; Houdek, M. T. Intrinsic tendon regeneration after application of purified

exosome product: An *in vivo* study. *Orthop. J. Sports Med*. **2021**, *9*, 23259671211062929.
[20] Shi, G. D.; Wang, Y. C.; Wang, Z. W.; Thoreson, A. R.; Jacobson, D. S.; Amadio, P. C.; Behfar, A.; Moran, S. L.; Zhao, C. F. A novel engineered purified exosome product patch for tendon healing: An explant in an *ex vivo* model. *J. Orthop. Res.* **2021**, *39*, 1825–1837.
[21] Wang, Y. C.; Shi, G. D.; Huang, T. C. T.; Li, J. L.; Long, Z. L.; Reisdorf, R.; Shin, A. Y.; Amadio, P.; Behfar, A.; Zhao, C. F. et al. Enhancing functional recovery after segmental nerve defect using nerve allograft treated with plasma-derived exosome. *Plast. Reconstr. Surg.* **2023**, *152*, 1247–1258.
[22] Mazzucchelli, L.; Sarcon, A. K.; Huang, T. C. T.; Li, J. L.; Berry, C. E.; Houdek, M. T.; Behfar, A.; Zhao, C. F.; Moran, S. L. A ready-to-use purified exosome product for volumetric muscle loss and functional recovery. *Tissue Eng. Part A* **2023**, *29*, 481–490.
[23] Xuan, W. X.; Wang, S. H.; Alarcon-Calderon, A.; Bagwell, M. S.; Para, R.; Wang, F. P.; Zhang, C. J.; Tian, X.; Stalboerger, P.; Peterson, T. et al. Nebulized platelet-derived extracellular vesicles attenuate chronic cigarette smoke-induced murine emphysema. *Transl. Res.* **2024**, *269*, 76–93.
[24] Zamanian, C.; Onyedimma, C.; Moinuddin, F. M.; Ghaith, A. K.; Jarrah, R.; Dhar, A.; Windebank, A. J.; Bydon, M. Evaluating purified exosome product and its role in neurologic and functional recovery following spinal cord injury in female rats. *J. Spinal Cord Med.* **2025**, *48*, 527–535.
[25] Pumford, A. D.; Staricha, K. L.; Kunkel, E. T.; Armstrong, M. F.; Behfar, A.; Van Abel, K. M. Exosome therapy for a nonhealing scalp wound following chemoradiation and surgical therapy. *Mayo Clin. Proc.* **2024**, *99*, 1006–1012.
[26] Rizzo, S. A.; Bagwell, M. S.; Schiebel, P.; Rolland, T. J.; Mahlberg, R. C.; Witt, T. A.; Nagel, M. E.; Stalboerger, P. G.; Behfar, A. Pulmonary biodistribution of platelet-derived regenerative exosomes in a porcine model. *Int. J. Mol. Sci.* **2024**, *25*, 2642.
[27] Coelho-Rato, L. S.; Parvanian, S.; Modi, M. K.; Eriksson, J. E. Vimentin at the core of wound healing. *Trends Cell Biol.* **2024**, *34*, 239–254.
[28] Behfar, A.; Terzic, A. *Rion PEP* [Online]. Rion Therapeutics: Rion Therapeutics, 2025. https://riontx.com/ (accessed Jul 17, 2025).
[29] Miller, C. M.; Enninga, E. A. L.; Rizzo, S. A.; Phillipps, J.; Guerrero-Cazares, H.; Destephano, C. C.; Peterson, T. E.; Stalboerger, P. G.; Behfar, A.; Khan, Z. Platelet-derived exosomes induce cell proliferation and wound healing in human endometrial cells. *Regen. Med.* **2022**, *17*, 805–817.
[30] Rademakers, D. J.; Saffari, S.; Saffari, T. M.; Pulos, N.; Shin, A. Y. The effect of local purified exosome product, stem cells, and tacrolimus on neurite extension. *J. Hand Surg. Am.* **2024**, *49*, 237–246.
[31] Saffari, S.; Rademakers, D. J.; Pulos, N.; Shin, A. Y. Dose-response analysis after administration of a human platelet-derived exosome product on neurite outgrowth *in vitro*. *Biotechnol. Bioeng.* **2023**, *120*, 3191–3199.
[32] Shi, G. D.; Long, Z. L.; De la Vega, R. E.; Behfar, A.; Moran, S. L.; Evans, C.; Zhao, C. F. Purified exosome product enhances chondrocyte survival and regeneration by modulating inflammation and promoting chondrogenesis. *Regen. Med.* **2023**, *18*, 55–71.
[33] Murphy, D. E.; de Jong, O. G.; Brouwer, M.; Wood, M. J.; Lavieu, G.; Schiffelers, R. M.; Vader, P. Extracellular vesicle-based therapeutics: Natural versus engineered targeting and trafficking. *Exp. Mol. Med.* **2019**, *51*, 32.
[34] Xia, Y. T.; Zhang, J. Z.; Liu, G.; Wolfram, J. Immunogenicity of extracellular vesicles. *Adv. Mater.* **2024**, *36*, 2403199.
[35] Wolfram, J.; Yang, Y.; Shen, J. L.; Moten, A.; Chen, C. Y.; Shen, H. F.; Ferrari, M.; Zhao, Y. L. The nano-plasma interface: Implications of the protein corona. *Colloids Surf. B: Biointerfaces* **2014**, *124*, 17–24.
[36] Ghebosu, R. E.; Pendiuk Goncalves, J.; Wolfram, J. Extracellular vesicle and lipoprotein interactions. *Nano Lett.* **2024**, *24*, 1–8.
[37] Samuelsson, E.; Shen, H. F.; Blanco, E.; Ferrari, M.; Wolfram, J. Contribution of Kupffer cells to liposome accumulation in the liver. *Colloids Surf. B: Biointerfaces* **2017**, *158*, 356–362.
[38] Chen, X. J.; Jiang, K.; Ferguson, C. M.; Tang, H.; Zhu, X. Y.; Lerman, A.; Lerman, L. O. Augmented efficacy of exogenous extracellular vesicles targeted to injured kidneys. *Signal Transduct. Target Ther.* **2020**, *5*, 199.
[39] Li, L.; Liu, H. M.; Wang, H. H.; Mao, Y.; Song, L. G.; Kang, Z. Q. Diabetic kidney disease progression alleviated in mice by ALKBH5-mediated UC-MSCs-derived exosomes that inhibit TRAF6 m6A modification and promote M2 macrophage polarisation. *Endocrinol. Diabetes Metab.* **2026**, *9*, e70131.
[40] FirstWorld PHARMA. *ILIAS Biologics Receives HREC Approval to Initiate First-in-Human Clinical Trial Evaluating Exosome Therapeutics ILB-202, the Treatment for CSA-AKI* [Online]. 2022. https://firstwordpharma.com/story/5543467 (accessed Jan 20, 2026).
[41] Hyun, S.; Choi, H.; Sub, Y.; Hong, D.; Ahn, S. H.; Choi, K.; Ryu, S.; Kim, Y.; Park, C.; Gee, H. Y. et al. Safety and anti-inflammatory effects of engineered extracellular vesicles (ILB-202) for NF-κB inhibition: A double-blind, randomized, placebo-controlled phase 1 trial. *J. Extracell. Vesicles* **2025**, *14*, e70141.
[42] Patel, H. A.; Wang, J. X.; Zinn, C. J.; Learmonth, M.; Lerman, L. O.; Wolfram, J.; Hickson, L. J. Fortifying the diabetic kidney disease treatment armamentarium: Multitarget senotherapeutic and regenerative strategies. *J. Am. Soc. Nephrol.* **2025**, *36*, 1655–1658.
[43] Alatta, L. S.; Elhusseiny, K. M.; Dietz, A. B.; Herrmann, S. M.; Lorenz, E. C.; Lawson, D. K.; Bendel, E. C.; Reisenauer, C. J.; Misra, S.; Vaughan, L. E. et al. Intraarterial autologous mesenchymal stem cell therapy for diabetic kidney disease. *Kidney Int. Rep.* **2025**, *10*, 3656–3660.
[44] Perico, N.; Remuzzi, G.; Griffin, M. D.; Cockwell, P.; Maxwell, A. P.; Casiraghi, F.; Rubis, N.; Peracchi, T.; Villa, A.; Todeschini, M. et al. Safety and preliminary efficacy of mesenchymal stromal cell (ORBCEL-M) therapy in diabetic kidney disease: A randomized clinical trial (NEPHSTROM). *J. Am. Soc. Nephrol.* **2023**, *34*, 1733–1751.
[45] Packham, D. K.; Fraser, I. R.; Kerr, P. G.; Segal, K. R. Allogeneic mesenchymal precursor cells (MPC) in diabetic nephropathy: A randomized, placebo-controlled, dose escalation study. *EBioMedicine* **2016**, *12*, 263–269.
[46] Van Delen, M.; Derdelinckx, J.; Wouters, K.; Nelissen, I.; Cools, N. A systematic review and meta-analysis of clinical trials assessing safety and efficacy of human extracellular vesicle-based therapy. *J. Extracell. Vesicles* **2024**, *13*, e12458.
[47] Mayo Clinic. *Safety and Tolerability of Vertebral Bone Marrow-derived Mesenchymal Stem Cells (BM-MSC) in Real World Scenarios of Patients with Chronic Kidney Disease (CKD)* [Online]. 2024; https://www.clinicaltrials.gov/study/NCT06752577 (accessed Jan 12, 2026).
[48] Nassar, W.; El-Ansary, M.; Sabry, D.; Mostafa, M. A.; Fayad, T.; Kotb, E.; Temraz, M.; Saad, A. N.; Essa, W.; Adel, H. Umbilical cord mesenchymal stem cells derived extracellular vesicles can safely ameliorate the progression of chronic kidney diseases. *Biomater. Res.* **2016**, *20*, 21.
[49] Kou, M.; Huang, L.; Yang, J. J.; Chiang, Z.; Chen, S. X.; Liu, J.; Guo, L. Y.; Zhang, X. X.; Zhou, X. Y.; Xu, X. et al. Mesenchymal stem cell-derived extracellular vesicles for immunomodulation and regeneration: A next generation therapeutic tool. *Cell Death Dis.* **2022**, *13*, 580.
[50] Iannotta, D.; Yang, M.; Celia, C.; Di Marzio, L.; Wolfram, J. Extracellular vesicle therapeutics from plasma and adipose tissue. *Nano Today* **2021**, *39*, 101159.
[51] Mizenko, R. R.; Feaver, M.; Bozkurt, B. T.; Lowe, N.; Nguyen, B.;

Huang, K. W.; Wang, A. J.; Carney, R. P. A critical systematic review of extracellular vesicle clinical trials. *J. Extracell. Vesicles* **2024**, *13*, e12510.

[52] Clinical Testing of Beverly Hills. *Purified Exosome Product* (*PEP*) *Injected Into the Hypodermis* (*PEP*) [Online]. 2025. https://clinicaltrials.gov/study/NCT06429033 (accessed Jan 20, 2026).

[53] McGraw, I. T.; Wilson, E. E.; Behfar, A.; Paradise, C. R.; Rohrich, R. J.; Wyles, S. P. Evolving role of exosomes in plastic and reconstructive surgery and dermatology. *Plast. Reconstr. Surg. Glob. Open* **2024**, *12*, e6061.

[54] Proffer, S. L.; Paradise, C. R.; DeGrazia, E.; Halaas, Y.; Durairaj, K. K.; Somenek, M.; Sivly, A.; Boon, A. J.; Behfar, A.; Wyles, S. P. Efficacy and tolerability of topical platelet exosomes for skin rejuvenation: Six-week results. *Aesthet. Surg. J.* **2022**, *42*, 1185–1193.

[55] Wyles, S. P.; Proffer, S. L.; Farris, P.; Randall, L.; Hillestad, M. L.; Lupo, M. P.; Behfar, A. Effect of topical Human Platelet Extract (HPE) for facial skin rejuvenation: A histological study of collagen and elastin. *J. Drugs Dermatol.* **2024**, *23*, 735–740.

[56] Elhusseiny, K. M.; Deceus, F. G.; Cornell, L. D.; Bian, X. H.; Ma, Y. H.; Kachergus, J. M.; Thompson, E. A.; Hickson, L. J. Capturing the inflammatory landscape within kidney compartments of human diabetic kidney disease: A digital spatial profiling study. *Front. Endocrinol.* **2026**, *17*, 1744430.

[57] Dorronsoro, A.; Santiago, F. E.; Grassi, D.; Zhang, T. P.; Lai, R. C.; McGowan, S. J.; Angelini, L.; Lavasani, M.; Corbo, L.; Lu, A. P. et al. Mesenchymal stem cell-derived extracellular vesicles reduce senescence and extend health span in mouse models of aging. *Aging Cell* **2021**, *20*, e13337.

[58] Kim, S. R.; Zou, X. Y.; Tang, H.; Puranik, A. S.; Abumoawad, A. M.; Zhu, X. Y.; Hickson, L. J.; Tchkonia, T.; Textor, S. C.; Kirkland, J. L. et al. Increased cellular senescence in the murine and human stenotic kidney: Effect of mesenchymal stem cells. *J. Cell. Physiol.* **2021**, *236*, 1332–1344.

[59] Li, X. Y.; Guo, L.; Chen, J. G.; Liang, H. W.; Liu, Y.; Chen, W.; Zhou, L.; Shan, L. T.; Wang, H. Intravenous injection of human umbilical cord-derived mesenchymal stem cells ameliorates not only blood glucose but also nephrotic complication of diabetic rats through autophagy-mediated anti-senescent mechanism. *Stem Cell Res. Ther.* **2023**, *14*, 146.

[60] Hickson, L. J.; Abedalqader, T.; Ben-Bernard, G.; Mondy, J. M.; Bian, X. H.; Conley, S. M.; Zhu, X. Y.; Herrmann, S. M.; Kukla, A.; Lorenz, E. C. et al. A systematic review and meta-analysis of cell-based interventions in experimental diabetic kidney disease. *Stem Cells Transl. Med.* **2021**, *10*, 1304–1319.

[61] Beetler, D. J.; Giresi, P.; Di Florio, D. N.; Fliess, J. J.; McCabe, E. J.; Watkins, M. M.; Xu, V.; Auda, M. E.; Bruno, K. A.; Whelan, E. R. et al. Therapeutic effects of platelet-derived extracellular vesicles on viral myocarditis correlate with biomolecular content. *Front. Immunol.* **2025**, *15*, 1468969.